



Surface wave resonance and chirality in a tubular cavity with metasurface design



Yuzhou Qin ^a, Yangfu Fang ^a, Lu Wang ^a, Shiwei Tang ^b, Shulin Sun ^c, Zhaowei Liu ^d,
Yongfeng Mei ^{a,*}

^a Department of Materials Science, State Key Laboratory of ASIC and Systems, Fudan University, Shanghai, 200433, China

^b Department of Physics, Faculty of Science, Ningbo University, Ningbo, 315211, China

^c Department of Optical Science and Engineering, Key Laboratory of Micro and Nano Photonic Structures (Ministry of Education), Fudan University, Shanghai, 200433, China

^d Department of Electrical and Computer Engineering, University of California, San Diego, CA 92093, USA

ARTICLE INFO

Keywords:

Tubular cavity
Optical resonance
Chirality
Surface wave
Whispering gallery mode
Metasurface

ABSTRACT

Optical microcavities with whispering-gallery modes (WGMs) have been indispensable in both photonic researches and applications. Besides, metasurfaces, have attracted much attention recently due to their strong abilities to manipulate electromagnetic waves. Here, combining these two optical elements together, we show a tubular cavity can convert input propagating cylindrical waves into directed localized surface waves (SWs), enabling the circulating like WGMs along the wall surface of the designed tubular cavity. Finite element method (FEM) simulations demonstrate that such near-field WGM shows both large chirality and high local field. This work may stimulate interesting potential applications in e.g. directional emission, sensing, and lasing.

1. Introduction

Optical microcavities have attracted much attention due to their potential applications in various fields, such as ultra-small optical filters, high-efficiency light emission diodes, low threshold lasers, nonlinear optics and quantum information processing [1–6]. Whispering gallery mode (WGM) resonators have attracted increasing interests due to their excellent performance and simple fabrication in geometry [7–9]. Via rolled-up technology, tubular WGM resonators show unique potential in both fabrication and application [7,10–14]. In a traditional WGM cavity, the propagating waves (PWs) of clockwise (CW) and counterclockwise (CCW) are coupled together and equal in their properties (e.g. amplitude, polarization and phase) in the presence of backscattering. However, the balance between CW and CCW can be broken due to explicit symmetry breaking, including asymmetrical scattering [15] and special cavity design [16,17], and spontaneous symmetry breaking, including optical nonlinearity [18,19]. Therefore, the chirality is commonly treated as the consequence from the difference between the CW and CCW components [15–17,19–22]. On the other hand, metasurface, formed by flat optical microstructures with carefully tailored radiation amplitude and phase distributions in subwavelength scale, has attracted great interest of photonic researches recently [23–32]. A reflection typed metasurface has been reported to be able to

serve as a new bridge to convert a propagating wave to a surface wave (SW) with high efficiency, which is verified by experiments from microwave [33] to optical regimes [34].

Here, we propose a tubular cavity with metasurface design under the illumination of cylindrical electromagnetic (EM) waves excited from a line source inside at microwave regime. Replacing the wall of tubular cavity by metasurface, a chiral SW-based WGM resonance is achieved by our structure rather than conventional WGM resonance. The chirality of WGM is solely determined by the phase gradient provided by the designed metasurface. Moreover, we suggest a multilayer structure to guide the inner SWs flowing outside the tubular cavity, achieving higher conversion efficiency and quality factor (Q factor). These studies may inspire potential applications on the enhanced light-matter interactions.

2. Results and discussion

2.1. Structure and characteristic of tubular cavity

The general structure of our tubular cavity is shown in Fig. 1(a). A layer of metal is put at the outside of a dielectric tubular cavity, while various pre-designed metallic blocks are put at inner surface of the tube. This metal–insulator–metal structure presents unique characteristic as metasurface. According to the previous research, the phase gradient is

* Corresponding author.

E-mail address: yfm@fudan.edu.cn (Y. Mei).

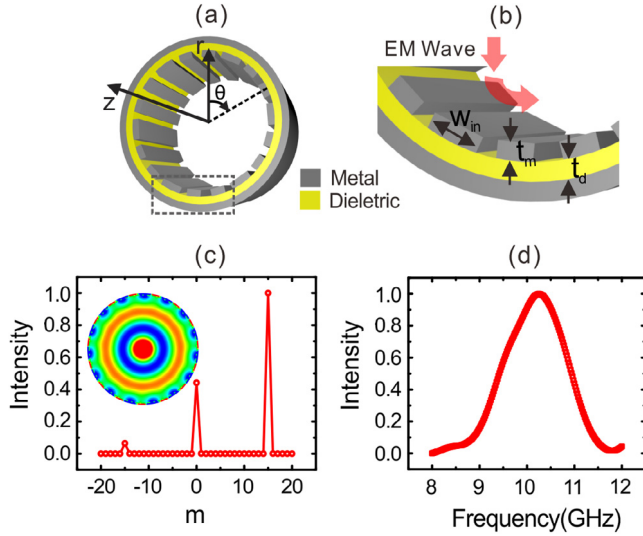


Fig. 1. General structure and characteristic of the tubular cavity with metasurface design. (a) Schematic diagram of tubular cavity. (b) The detailed structure of the supercell. Four metallic blocks are evenly distributed in a supercell. Here the length of the supercell is set as 20 mm. And the widths of metallic blocks w_{in} are set as 1.2 mm, 2.9 mm, 3.2 mm and 4 mm, respectively. And the thicknesses of the layers t_m and t_d are as 0.6 mm and 1.2 mm. (c) The calculated normalized angular momentum distribution at the working frequency $f = 10$ GHz of the tubular cavity. The positive and negative mode numbers correspond to CW and CCW components, respectively. The H_z field distribution is shown in the inset. (d) The average intensities around the inner surface of the tubular cavity at the working frequency $f = 10$ GHz.

designed as ξ in the metasurface [33]. Assuming that the metasurface is illuminated by the incident wave along the radial direction, it can be obtained that the tangential wave vector $k_t = \xi$. The cylindrical wave is produced by a transverse magnetic (TM) line source which was put at the center of the tube with the magnetic field along the axial direction.

The wall of tubular cavity is divided into 15 supercells. The detailed structure of a supercell is shown in Fig. 1(b). A supercell consists of a layer of dielectric between a metallic layer and a layer with four metallic blocks. The relative permittivity of the dielectric is set as $\epsilon = 10$. The metal is considered as perfect electric conductor (PEC) at microwave regime and the relative permittivity is set as infinite. Since both thickness of the dielectric and width of metallic blocks have similar influences in the reflection phase, we set the thickness of the dielectric is fixed as $t_d = 1.2$ mm, and the thickness of inner and outer metal is $t_m = 0.6$ mm. The width of the metallic blocks w_{in} in one supercell are set as 1 mm, 2.9 mm, 3.2 mm and 4 mm, respectively, which satisfy $\Delta\Phi = \pi/2$. The detail design process of the metasurface is shown in the supplementary material (Part S1 and S2).

Since the outer metallic layer acts as PEC in the microwave regime, the EM field is confined inside the tube. Through FEM simulation, the H_z field distributions are obtained and plotted in the inset of Fig. 1(c). Comsol Multiphysics software is applied for the two dimensional simulation process. The boundary is set as perfect matched layer (PML) and mesh size is fine enough comparing to the size of metallic blocks (the maximal 8 mm and the minimum 0.01 mm). As revealed in the field distribution, the PW is converted to the directional SW along the surface. In addition, the SW is periodical, which exactly agrees with the number of periods of the metasurface, showing the feature of WGM. It is noted that the WGM here is a driven state since the SWs are not the eigenmodes of the metasurface and are produced by PWs inside every individual supercell. Different from the traditional WGM resonator, the EM wave in our tubular metasurface travels along the inner surface forming the driven-WGM rather than experiences totally reflection in the dielectric layer. Due to the predesigned phase gradient direction,

the SW propagates in a specialized direction. As a result, the intensity of CW waves and CCW waves will be different, leading to the uni-chirality of the cavity.

By solving the Helmholtz equation, the wave functions inside the cavity can be expanded in cylindrical harmonics

$$\Psi(\rho, \varphi) = \sum_{m=-\infty}^{+\infty} a_m J_m(nk\rho) \exp(im\varphi), \quad (1)$$

where m is the quantum number of angular momentum. Parameter k is the wave vector. ρ and φ are coordinates in the polar coordinate system. J_m is the m th order Bessel function, and a_m is corresponding coefficient. The calculated normalized angular momentum distribution at the working frequency of the metasurface is plotted in Fig. 1(c). Positive and negative values of the angular momentum mode number m correspond to the CW and CCW propagating components, respectively. It is to be noted that the positive and negative values of the same azimuthal mode index represent same mode index of CW and CCW components along the inner surface, respectively. The intensity difference between the CW and CCW components indicates chirality in the cavity. Defining the chirality of the tubular cavity as

$$\alpha = 1 - \frac{\min\{\sum_{m=-\infty}^{m=-1} |a_m|^2, \sum_{m=1}^{m=\infty} |a_m|^2\}}{\max\{\sum_{m=-\infty}^{m=-1} |a_m|^2, \sum_{m=1}^{m=\infty} |a_m|^2\}}, \quad (2)$$

the chirality is approximately 0.935. Therefore, the intensity of CW component is much larger than CCW component, demonstrating that our structure can produce a chiral EM wave with high efficiency.

According to the field distribution, we could achieve the PW–SW conversion efficiency as approximately 80% since the radial modes formed by scattering loss.

As shown in Fig. 1(d), we obtain the average intensities around the inner surface of the tubular cavity. When the SW propagates along the surface and satisfies $2\pi R = m\lambda_{SW}$, it is similar to the PW in the normal WGM cavity and resonates at a certain frequency. Besides, the frequency should not only satisfy the tubular resonator but also be consistent with the working frequency of the metasurface. As a result, the WGM only exists when the mode number exactly equals to the number of periods. Since the phase gradient only exists at the specialized frequency, then the intensity increases greatly at the working frequency.

2.2. Structure and characteristic of tubular cavity based on transmission model

Considering that the SW based WGM is only a driven state under the illuminance of input EM wave, the SWs experience significant scattering between the supercells and leading to high loss and low conversion efficiency. Therefore, we replace the outside PEC by periodic metallic blocks to convert the SWs to be the eigenmode of the metasurface. It is also worthwhile to note that the distribution of transmission phase should be large enough to maintain the phase gradient when we lead the SW to the outside. Therefore, a multilayer structure is applied to expand the range of transmission phase, as shown in Fig. 2(a). The detail design process is shown in the supplementary material (Part S3). As a result, we set w_{in} in one unit as 0.2, 3.6, 3.2 and 4.5 mm respectively, while w_{mid} blocks are set in one unit as 1, 2, 4, 4.8 and 4.8 mm respectively, and w_{out} is set as 4 mm in every supercell for the chosen frequency 10 GHz. The thicknesses of metallic layers t_m are set as 0.6 mm, while the dielectric layers t_d are 1.2 mm. Applying such structure, the H_z field distribution is achieved through FEM simulation and plotted in Fig. 2(b). The field distribution also reveals WGM produced by the SW on the outer surface, which is similar to the reflection model. Besides, the EM wave travels around the outer surface of the tube as SW in certain direction, and the radiation loss is compressed. The PW–SW conversion is 98% due to the suppression of the radial mode formed by the scattering wave.

Similarly the wave functions inside the cavity can be expanded in cylindrical harmonics as

$$\Psi(\rho, \varphi) = \sum_{m=-\infty}^{+\infty} b_m H_m^{(2)}(nk\rho) \exp(im\varphi), \quad (3)$$

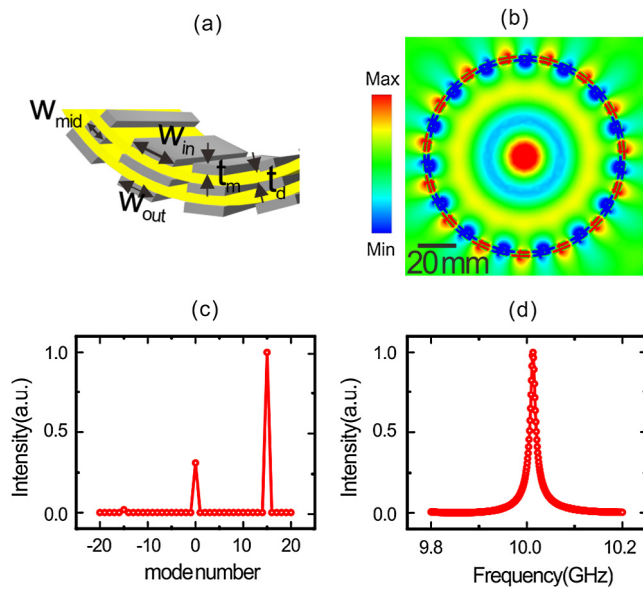


Fig. 2. General structure and characteristic of the transmission model of the tubular cavity. (a) The structure of a supercell in the transmission model. The whole structure consists of two layers of dielectric (yellow) between three layers of metallic blocks (gray). The thickness of the dielectric layers t_d is 1.2 mm, while the thickness of the metallic layers t_m is 1.2 mm. The width of the metallic blocks w_{out} is fixed as 4 mm, w_{in} is set as 0.2, 3.6, 3.2, and 4.5 mm, respectively while w_{mid} are 1, 2, 4, 4.8 mm, respectively. (b) The H_z field distribution of the transmission model. (c) The calculated normalized angular momentum distribution at the working frequency $f = 10$ GHz of the tubular cavity. The positive and negative mode numbers correspond to CW and CCW components, respectively. (d) The average intensity around the outer surface of the tubular cavity. (For interpretation of the references to color in this figure legend, the reader is referred to the web version of this article.)

where $H_m^{(2)}$ is the second kind m th order Hankel function. The normalized angular momentum distribution is plotted in Fig. 2(c). Strong chirality is represented due to the great contrast between the intensities in $m = 15$ and $m = -15$ modes. The calculated chirality is approximately 0.983 according to Eq. (2).

Fig. 2(d) shows the average intensity around the outer surface of the tube. This result shows that the SW propagates around the outer surface and forms a WGM cavity, showing the combination of the directional SW and the WGM cavity. The resonance frequency deviates from the working frequency due to the influence of the inner and middle layers to the eigenmodes. Besides, the less loss of the SW leads to higher Q factor (around 700) of the WGM cavity. Hence, our structure reveals the enhancement of electromagnetic field as a cavity and have potential in acting as functional plasmonic lasers.

2.3. Guiding out SW with mushroom structure

In order to guide out the SW outside the tubular cavity, we design a mushroom structure to support the SW as eigen spoof SPP at the working frequency for the coupling. The schematic structure is sketched in Fig. 3(a). Microwave can propagate along the mushroom structure with low loss [35]. The detailed design process of the mushroom structure is shown in supplementary material (Part S4). Via placing the mushroom structure near the tubular cavity, the CW and CCW components can be led to opposite sides of the mushroom structure. The average field intensity at the opposite sides on the mushroom structure is also obtained and shown in Fig. 3(b). The CW and CCW components show great intensity difference at the working frequency $f = 10$ GHz of the metasurface, which means the mushroom structure is indeed the best candidate to guide the chiral SW out. The H_z field

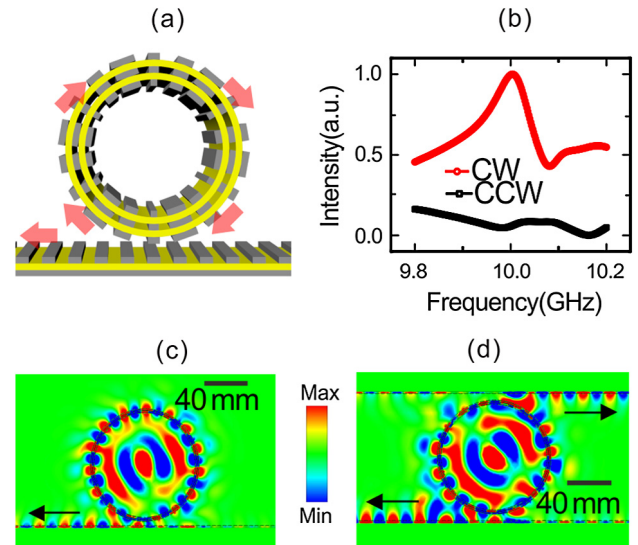


Fig. 3. Coupling the mushroom structure to guide out the SW. (a) The schematic structure of the tubular cavity with the neighbor mushroom structure. (b) The average field intensity at the opposite sides on the mushroom structure. (c) The H_z field distribution of tubular cavity with mushroom structure at one side. (d) The H_z field distribution of tubular cavity with mushroom structure at the opposite side.

distribution at the working frequency $f = 10$ GHz is revealed in Fig. 3(c). Loss exists in the coupling process and the efficiency is approximately 91%. When coupled by the mushroom structure, the SW can only propagate in the direction which aligns with the predefined direction of the metasurface. Thus the EM wave from the isotropic source can be converted to SW in a specialized direction.

We then put the mushroom structure at the both opposite sides of the tubular cavity. The corresponding H_z field distribution is shown in Fig. 3(d). The tubular cavity, which acts as a beam splitter, leads the SW to opposite directions at corresponding mushroom structures (upper and down). The directions of mushroom structures can be easily changed to yield SW with different orientations at the same time.

Besides, the tubular cavity with metasurface design could be fabricated through curved PCB with grating structure in different widths for microwave regime in experiment. Meanwhile, our design could extend to visible regime through the rolling of nanopatterned nanomembranes [36,37].

3. Conclusion

To summarize, a tubular cavity with metasurface design is proposed, working at microwave regime. Under the illumination of a cylindrical wave, the tubular cavity could couple the SW along its inner surface, achieving a SW-based WGM resonance. The predefined phase gradient of the metasurface leads to uni-chirality of the SW-based WGM. Moreover, we couple the inner SW flowing outside the tubular cavity by using designed metallic structures instead of the PEC layer and realize a SW-based WGM high Q factor and high PW–SW conversion efficiency. Coupling mushroom structure to the tubular cavity, a SW-based WGM and directional SW is numerically demonstrated by FEM simulations. Therefore, combining both high Q factor and strong chirality comparing to other WGM or flat structure, our results might stimulate potential applications in such as near-field sensing, functional plasmonic circuitry and lasers.

See supplementary material for the design of the tubular cavity and the robustness of chirality.

Acknowledgments

This work is supported by the Natural Science Foundation of China (51322201, 61628401, 11604167, U1632115), Science and Technology Commission of Shanghai Municipality (17JC1401700), National Basic Research Program of China (2017YFA0303500) and the Changjiang Young Scholars Program of China.

Appendix A. Supplementary material

Supplementary material related to this article can be found online at <https://doi.org/10.1016/j.optcom.2018.02.011>.

References

- [1] S. Noda, A. Chutinan, M. Imada, Trapping and emission of photons by a single defect in a photonic bandgap structure, *Nature* 407 (2000) 608–610.
- [2] P. Michler, A. Kiraz, C. Becher, W.V. Schoenfeld, P.M. Petroff, L. Zhang, E. Hu, A. Imamoglu, A quantum dot single-photon turnstile device, *Science* 290 (2000) 2282–2285.
- [3] B.-S. Song, S. Noda, T. Asano, Y. Akahane, Ultra-high-Q photonic double-heterostructure nanocavity, *Nature Mater.* 4 (2005) 207–210.
- [4] M. Qiu, B. Jaskorzynska, Design of a channel drop filter in a two-dimensional triangular photonic crystal, *Appl. Phys. Lett.* 83 (2003) 1074–1076.
- [5] O. Painter, R.K. Lee, A. Scherer, A. Yariv, J.D. O'Brien, P.D. Dapkus, I. Kim, Two-dimensional photonic band-gap defect mode laser, *Science* 284 (1999) 1819–1821.
- [6] S.M. Spillane, T.J. Kippenberg, K.J. Vahala, Ultralow-threshold Raman laser using a spherical dielectric microcavity, *Nature* 415 (2002) 621–623.
- [7] J. Wang, T. Zhan, G. Huang, P.K. Chu, Y. Mei, Optical microcavities with tubular geometry: properties and applications, *Laser Photonics Rev.* 8 (2014) 521–547.
- [8] K.J. Vahala, Optical microcavities, *Nature* 424 (2003) 839–846.
- [9] A.M. Armani, R.P. Kulkarni, S.E. Fraser, R.C. Flagan, K.J. Vahala, Label-free, single-molecule detection with optical microcavities, *Science* 317 (2007) 783–787.
- [10] Y. Mei, G. Huang, A.A. Solovev, E.B. Urena, I. Moench, F. Ding, T. Reindl, R.K.Y. Fu, P.K. Chu, O.G. Schmidt, Versatile approach for integrative and functionalized tubes by strain engineering of nanomembranes on polymers, *Adv. Mater.* 20 (2008) 4085–4090.
- [11] S. Tang, Y. Fang, Z. Liu, L. Zhou, Y. Mei, Tubular optical microcavities of indefinite medium for sensitive liquid refractometers, *Lab Chip* 16 (2016) 182–187.
- [12] Y. Fang, S. Li, Y. Mei, Modulation of high quality factors in rolled-up microcavities, *Phys. Rev. A* 94 (2016) 33804.
- [13] J. Wang, T. Zhan, G. Huang, X. Cui, X. Hu, Y. Mei, Tubular oxide microcavity with high-index-contrast walls: Mie scattering theory and 3D confinement of resonant modes, *Opt. Express* 20 (2012) 18555–18567.
- [14] Y. Lan, S. Li, Z. Cai, Y. Mei, S. Kiravittaya, Semi-analytical calculation of resonant modes in axially asymmetric microtube resonators, *Opt. Commun.* 386 (2017) 72–76.
- [15] J. Zhu, S.K. Ozdemir, Y.-F. Xiao, L. Li, L. He, D.-R. Chen, L. Yang, On-chip single nanoparticle detection and sizing by mode splitting in an ultrahigh-Q microresonator, *Nat. Photonics* 4 (2010) 46–49.
- [16] Q. Song, N. Zhang, H. Zhai, S. Liu, Z. Gu, K. Wang, S. Sun, Z. Chen, M. Li, S. Xiao, The combination of high Q factor and chirality in twin cavities and microcavity chain, *Sci. Rep.* 4 (2014) 6493.
- [17] J. Wiersig, A. Eberspächer, J.B. Shim, J.W. Ryu, S. Shinohara, M. Hentschel, H. Schomerus, Nonorthogonal pairs of copropagating optical modes in deformed microdisk cavities, *Phys. Rev. A* 84 (2011) 23845.
- [18] X. Jiang, L. Shao, S.X. Zhang, X. Yi, J. Wiersig, L. Wang, Q. Gong, M. Loncar, L. Yang, Y.F. Xiao, Chaos-assisted broadband momentum transformation in optical microresonators, *Science* 358 (2017) 344–347.
- [19] Q.T. Cao, H. Wang, C.H. Dong, H. Jing, R.S. Liu, X. Chen, L. Ge, Q. Gong, Y.F. Xiao, Experimental demonstration of spontaneous chirality in a nonlinear microresonator, *Phys. Rev. Lett.* 118 (2017) 1–5.
- [20] J. Wiersig, S.W. Kim, M. Hentschel, Asymmetric scattering and nonorthogonal mode patterns in optical microspirals, *Phys. Rev. A* 78 (2008) 53809.
- [21] M. Kim, A.M.H. Wong, G.V. Eleftheriades, Optical Huygens' metasurfaces with independent control of the magnitude and phase of the local reflection coefficients, *Phys. Rev. X* 4 (2014) 41042.
- [22] B. Peng, Ş.K. Özdemir, M. Liertzer, W. Chen, J. Kramer, H. Yilmaz, J. Wiersig, S. Rotter, L. Yang, Chiral modes and directional lasing at exceptional points, *Proc. Natl. Acad. Sci.* 113 (2016) 201603318.
- [23] N. Yu, F. Capasso, Flat optics with designer metasurfaces, *Nature Mater.* 13 (2014) 139–150.
- [24] C.L. Holloway, E.F. Kuester, J.A. Gordon, J. O'Hara, J. Booth, D.R. Smith, An overview of the theory and applications of metasurfaces: The two-dimensional equivalents of metamaterials, *IEEE Antennas Propag. Mag.* 54 (2012) 10–35.
- [25] S.B. Glybovski, S.A. Tretyakov, P.A. Belov, Y.S. Kivshar, C.R. Simovski, Metasurfaces: From microwaves to visible, *Phys. Rep.* 634 (2016) 1–72.
- [26] H.-T. Chen, A.J. Taylor, N. Yu, A review of metasurfaces: physics and applications, *Rep. Progr. Phys.* 79 (2016) 76401.
- [27] H. Yang, Y. Deng, Broadband and high efficiency all-dielectric metasurfaces for wavefront steering with easily obtained phase shift, *Opt. Commun.* 405 (2017) 39–42.
- [28] H. Shao, C. Chen, J. Wang, L. Pan, T. Sang, Metalenses based on the non-parallel double-slit arrays, *J. Phys. D: Appl. Phys.* 50 (2017) 384001.
- [29] J.I.W. Ang, C.I.S. Ong, J.I.N.G.H. Ang, Z.A.H.U. Heng, F. Eng, Z. Hang, Tunable Fano resonance based on grating-coupled and graphene-based Otto configuration, *Opt. Express* 25 (2017) 183–191.
- [30] B. Tang, J. Wang, X. Xia, X. Liang, C. Song, S. Qu, Plasmonic-induced transparency and unidirectional control based on the waveguide structure with quadrant ring resonators, *Appl. Phys. Express* 8 (2015) 32202.
- [31] J. Zhou, H. Qian, G. Hu, H. Luo, S. Wen, Z. Liu, Broadband photonic spin hall metalens, *ACS Nano* 12 (2018) 82–88.
- [32] J. Zhou, W. Zhang, Y. Liu, Y. Ke, Y. Liu, H. Luo, S. Wen, Spin-dependent manipulating of vector beams by tailoring polarization, *Sci. Rep.* 6 (2016) 1–9.
- [33] S. Sun, Q. He, S. Xiao, Q. Xu, X. Li, L. Zhou, Gradient-index meta-surfaces as a bridge linking propagating waves and surface waves, *Nature Mater.* 11 (2012) 426–431.
- [34] S. Sun, K. Yang, C. Wang, T. Juan, W.T. Chen, C.Y. Liao, Q. He, S. Xiao, W. Kung, G. Guo, L. Zhou, D.P. Tsai, High-Efficiency broadband anomalous reflection by gradient meta-surfaces, *Nano Lett.* 12 (2012) 6223–6229.
- [35] M.J. Lockyear, A.P. Hibbins, J.R. Sambles, Microwave surface-plasmon-like modes on thin metamaterials, *Phys. Rev. Lett.* 102 (2009) 73901.
- [36] X. Lin, Y. Fang, L. Zhu, J. Zhang, G. Huang, J. Wang, Y. Mei, Self-rolling of oxide nanomembranes and resonance coupling in tubular optical microcavity, *Adv. Opt. Mater.* 4 (2016) 936–942.
- [37] Z. Tian, L. Zhang, Y. Fang, B. Xu, S. Tang, N. Hu, Z. An, Z. Chen, Y. Mei, Deterministic self-rolling of ultrathin nanocrystalline diamond nanomembranes for 3D tubular/helical architecture, *Adv. Mater.* 29 (2017) 1604572.